A DFT Study of the Amination of Fullerenes and Carbon Nanotubes: Reactivity and Curvature

Tingting Lin, Wei-De Zhang, Junchao Huang, and Chaobin He*

Institute of Materials Research and Engineering, 3 Research Link, Singapore 117602

Received: March 1, 2005; In Final Form: May 17, 2005

The first principles density functional theory (DFT) approach (GGA-PW91/DNP) was used to study the addition reaction of methylamine to fullerenes C_{50} and C_{60} or single-walled carbon nanotubes (SWNTs) (5,5) and (10,0). To understand the relationship between reactivity and curvature, various addition sites have been investigated for comparisons. The DFT calculation results showed that the reaction energy of the addition of methylamine onto C_{60} or the closed caps of (5,5) and (10,0) is rather low. Moreover, the reaction at a few sites even appears exothermic. However, the reaction on the perfect sidewall of the nanotubes is always endothermic, and the reaction energy is much higher than that on the caps. The energetically preferable addition sites are the carbon atoms located at the vertexes formed with five-, five-, six-membered rings on C_{50} or five-, five-, seven-membered rings on defects of nanotubes. The systematic theoretical study revealed that the pyramidalization and π-orbital misalignment could result in an increased reactivity of these pentagon−pentagon fusion sites. The reactivity depends on the pyramidalization angle, which is a quantitative measurement of the local curvature and strain of the reaction center.

Introduction

Functionalization of carbon nanotubes has drawn much attention from experimental and theoretical researchers[1,2] because of their potential applications in the areas of nanotube−polymer nanocomposites and nanotube-based sensors. The properties of fullerenes and carbon nanotubes are different from those of graphite because of their strained and nonplanar morphology. The curvature leads to a loss of spatial overlap of the atomic p orbitals and a shift in hybridization of the carbon atoms from the sp^2 of graphite to an intermediate state between sp^2 and sp^3. In general, the chemical reactivity of a fullerene or a single-walled carbon nanotube (SWNT) is governed by the local atomic arrangement of a reaction site. A pyramidalization angle (θ_p) was introduced to measure the deviation of a sp^2-hybridized carbon atom from the plane passing through the three adjacent carbon atoms. From the specific carbon atom, a vector is drawn so that it makes equal angles $\theta_{\sigma\pi}$ with the directions of the bonds with the three adjacent carbon atoms. Then, the pyramidalization angle is $\theta_p = \theta_{\sigma\pi} - 90°$.[3−5] The θ_p is 0° for a planar sp^2-hybridized carbon atom and about 19.5° for a sp^3-hybridized carbon atom. The local Gaussian curvature of the surface of a single fullerene or a single SWNT is related to θ_p by the equation $\kappa = 2 \sin \theta_p/a$, where a is the average distance to the adjacent atoms.[6] It was also found that the σ-strain energy is proportional to the square of θ_p[7] and so are the heats of formation of fullerenes obtained from MNDO calculations.[8] The objective of this work is to investigate the dependence of the reactivity on the pyramidalization angle by DFT computations.

An accurate determination of the mechanisms of SWNTs fuctionalization is, however, computationally extremely demanding because of the large number of atoms contained in such systems. In addition, the sidewall functionalization distorts the tube significantly. The use of any lower-level methods is not able to describe the bond breaking/forming. ONIOM is a computationally efficient tool for the study of chemical reactions involving large molecular systems. The two- or three-level ONIOM method divides a large molecular system into two or three sections. A relatively small section (model), essential for studying the properties of interest, is treated at a higher theoretical level (usually ab initio or DFT). The remaining one or two layers, serving mostly to constrain the general geometry, are described by a computationally less expensive method (molecular mechanics or semiempirical). However, calculations with ONIOM sometimes provided varying results, depending on the selection of the model size and the level of theory. The weakness may prevent the application of this approach from deriving reliably the functionalization of SWNTs.[9,10] Alternatively, if all the atoms in the molecular system are treated equally at the same theoretical level (DFT), more consistent computation results will be obtained.

The direct solvent-free amination of fullerenes and nanotubes has been investigated experimentally and calculated at the levels B3LYP/STO-3G and AM1 for C_{60}[11] and nanotubes,[12] respectively. In this work, fully DFT computations were performed at the level of GGA-PW91/DNP (fine) using DMol^3 software[13,14] to investigate the addition reaction of methylamine to the C_{50} and C_{60} fullerenes or the armchair (5,5) and zigzag (10,0) SWNTs. In addition to the regular sites at the tips and on the perfect sidewall, defect sites such as the 7−5−5−7 defect or the kink at the junction of two nanotubes were also investigated. Furthermore, the pyramidalization angles of carbon atoms of geometric optimized fullerenes or carbon nanotubes were analyzed and correlated to the reactivity of the sites.

Models and Computational Methods

Fullerenes C_{50} and C_{60}, and armchair (5,5) and zigzag (10,0) SWNTs were selected as the typical models because they are not only small in size but also exhibit curvature characteristics. Each end of the nanotubes in the models is either "open" (the

* Corresponding author. E-mail: cb-he@imre.a-star.edu.sg.

10.1021/jp051022g CCC: $30.25
Published on Web 06/24/2005

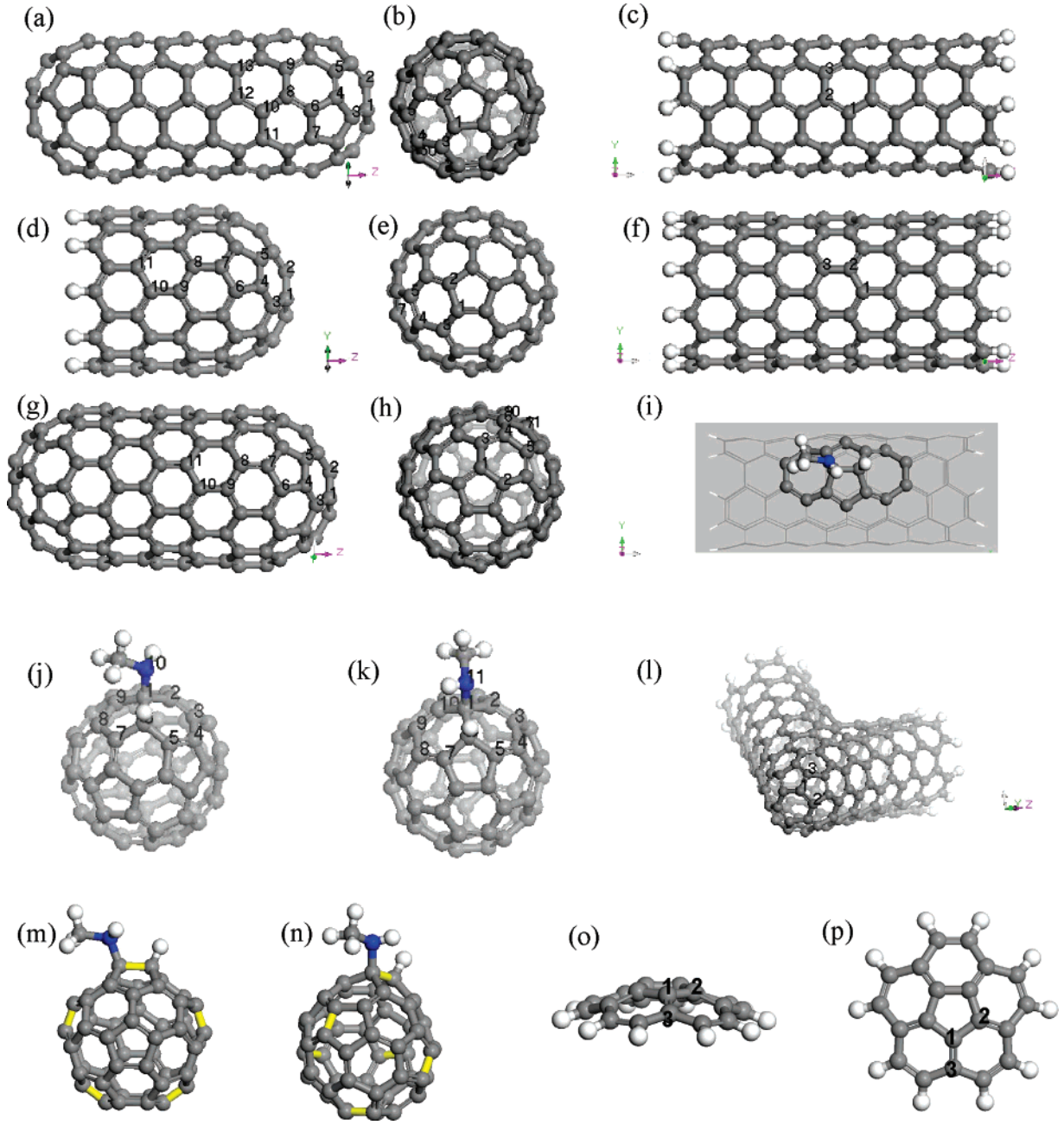

Figure 1. Fully DFT-optimized (at the level of theory GGA-PW91/DNP(fine)) structures and the atom numbering schemes. (a) side view and (b) top view of model **5_5_capsC$_{140}$**; (c) model **5_5C$_{140}$H$_{20}$**; (d) side view and (e) top view of model **10_0_capC$_{100}$H$_{10}$**; (f) model **10_0C$_{160}$H$_{20}$**; (g) side view and (h) top view of model **10_0_capsC$_{160}$**; methylamine addition via (i) the 5,5 bond on **5_5_d1**, (5,5) nanotube with a 7−5−5−7 defect on the sidewalls; (j) the 5,6 bond on **C$_{60}$(*I*$_h$)**; (k) the 6,6 bond on **C$_{60}$(*I*$_h$)**; (l) the 5,5 bond on **5_5_kink**, a joint of two tubes; (m) the 5,5 bonds (highlighted in yellow) on **C$_{50}$(*D*$_{5h}$)**; (n) the 5,5 bonds (highlighted in yellow) on **C$_{50}$(*D*$_3$)**; (o) side view and (p) top view of model **C$_{20}$H$_{10}$(bowl)**.

dangling bonds being saturated with hydrogen atoms) or "closed" with a half buckminsterfullerene C_{60}. Some models studied are shown in Figure 1. Figure 1a represents the side view and Figure 1b the top view of model **5_5_capsC$_{140}$**. The model is composed of a part of the (5,5) nanotube and two closed ends. It contains 140 carbon atoms. Figure 1c shows the model of **5_5C$_{140}$H$_{20}$**, a fragment of the (5,5) nanotube with two open ends. This model has 140 carbon atoms and 20 hydrogen atoms. Figure 1d shows the side view and Figure 1e the top view of model **10_0_capC$_{100}$H$_{10}$**, a shorter piece of the (10,0) nanotube. One of its ends is closed and the other end is open. Figure 1f illustrates the model of **10_0C$_{160}$H$_{20}$**, a longer piece of the (10,0) nanotube with two open ends. Figure 1g is the side view and Figure 1h the top view of model **10_0_capsC$_{160}$**, a fragment of the (10,0) nanotube with two closed ends.

Figure 1i represents for the methylamine addition via a bond fused with two five-membered rings (the 5,5 bond) on model **5_5_d1**, a section of the (5,5) nanotube with the 7−5−5−7 defect on the sidewall. Figures 1j and 1k show the optimized structures of the methylamine addition via a bond fused with a five-member and a six-member rings (the 5,6 bond) on model **C$_{60}$(*I*$_h$)** (C_{60} with symmetry I_h) and a bond fused with 2 six-member rings (the 6,6 bond) on **C$_{60}$(*I*$_h$)**, respectively. Figure 1l shows the model of **5_5_kink**, a hypothetical junction of two nanotubes. Figures 1m and 1n are the optimized structures of the methylamine addition via the 5,5 bond (highlighted in yellow, totally there are five such equatorial 5,5 bonds) on model **C$_{50}$(*D*$_{5h}$)** (an isomer of C_{50} with symmetry D_{5h}) and the 5,5 bond (highlighted in yellow, there are six 5,5 bonds altogether) on model **C$_{50}$(*D*$_3$)** (an isomer of C_{50} with symmetry D_3),

TABLE 1: Pyramidalization Angles θ_p (degree) and π-orbital Misalignment Angles ϕ (degree) at Molecular Geometries Fully Optimized Using DFT Method at the Level of GGA-PW91/DNP

site	C atom labels	vertex formed with n,m,l membered rings	pyramidalization angle θ_p	local curvature $\sin\theta_p$		misalignment angle ϕ
C_{60} (I_h)	1	5,6,6	11.64	0.202		0
			11.6,[a] 11.64[b,c]	0.201, 0.202		0[b]
C_{50}(D_{5h})	1	5,5,6	15.60	0.269	$\phi_{1,2}$	0.01
	2	5,5,6	15.53	0.268		
			15.5[a]	0.267		
C_{50}(D_3)	1	5,5,6	15.21	0.262	$\phi_{1,2}$	1.98
	2	5,5,6	14.15	0.244		
			15.2,[a] 14.0[a]	0.262, 0.242		
5_5$C_{140}H_{20}$	1	6,6,6	5.93	0.103	$\phi_{1,2}$	21.12
	2	6,6,6	5.98	0.104	$\phi_{1,3}$	−0.01
	3	6,6,6	5.85	0.102		
			5.97[b,c]	0.104		21.3,[b,c] 0[b,c]
10_0$C_{160}H_{20}$	1	6,6,6	5.18	0.090	$\phi_{1,2}$	0.00
	2	6,6,6	5.18	0.090	$\phi_{2,3}$	18.00
	3	6,6,6	5.20	0.091		
			5.15[b,c]	0.090		0,[b,c] 18.5[b,c]
5_5_capsC_{140}	1	5,6,6	11.89	0.206	$\phi_{1,2}$	0.03
	2	5,6,6	11.86	0.205	$\phi_{1,3}$	0.00
	3	5,6,6	12.12	0.210	$\phi_{3,4}$	0.27
	4	5,6,6	11.66	0.202	$\phi_{4,5}$	0.04
	5	5,6,6	11.63	0.202	$\phi_{4,6}$	2.25
	6	5,6,6	10.42	0.181	$\phi_{6,7}$	0.02
	7	5,6,6	10.45	0.181	$\phi_{6,8}$	10.19
	8	6,6,6	7.41	0.129	$\phi_{8,9}$	0.02
	9	6,6,6	7.44	0.129	$\phi_{8,10}$	18.68
	10	6,6,6	5.77	0.101	$\phi_{10,11}$	0.02
	11	6,6,6	5.87	0.102	$\phi_{10,12}$	21.49
	12	6,6,6	5.82	0.101	$\phi_{12,13}$	0.02
	13	6,6,6	5.70	0.099		
10_0_cap$C_{100}H_{10}$	1	5,6,6	10.58	0.184	$\phi_{1,2}$	0.00
	2	5,6,6	10.60	0.184	$\phi_{1,3}$	0.00
	3	6,6,6	9.06	0.157	$\phi_{3,4}$	−0.35
	4	5,6,6	10.76	0.187	$\phi_{4,5}$	0.03
	5	5,6,6	10.76	0.187	$\phi_{4,6}$	−0.79
	6	5,6,6	10.79	0.187	$\phi_{6,7}$	3.30
	7	5,6,6	9.20	0.160	$\phi_{7,8}$	0.06
	8	6,6,6	6.97	0.121	$\phi_{8,9}$	−17.21
	9	6,6,6	4.88	0.085	$\phi_{9,10}$	0.58
	10	6,6,6	5.02	0.088	$\phi_{10,11}$	−18.61
	11	6,6,6	4.65	0.081		
10_0capsC_{160}	1	5,6,6	10.59	0.184	$\phi_{1,2}$	−0.01
	2	5,6,6	10.60	0.184	$\phi_{1,3}$	0.02
	3	6,6,6	8.92	0.155	$\phi_{3,4}$	−0.28
	4	5,6,6	10.71	0.186	$\phi_{4,5}$	−0.07
	5	5,6,6	10.80	0.187	$\phi_{4,6}$	0.66
	6	5,6,6	10.78	0.187	$\phi_{6,7}$	3.10
	7	5,6,6	9.30	0.162	$\phi_{7,8}$	0.01
	8	6,6,6	6.77	0.118	$\phi_{8,9}$	−17.22
	9	6,6,6	5.01	0.087	$\phi_{9,10}$	0.68
	10	6,6,6	4.98	0.087	$\phi_{10,11}$	−18.72
	11	6,6,6	4.93	0.086		
5_5_d1 (7−5−5−7 defect)	1	5,5,7	15.80	0.272	$\phi_{1,2}$	0.00
	2	5,5,7	15.80	0.272		
5_5_kink	1	5,5,6	16.30	0.281	$\phi_{1,2}$	6.13
	2	5,6,6	12.98	0.225	$\phi_{1,3}$	0.04
	3	5,5,6	16.30	0.281		
$C_{20}H_{10}$(bowl)	1	5,6,6	8.34	0.145	$\phi_{1,2}$	0.01
	2	5,6,6	8.34	0.145	$\phi_{1,3}$	0.12
	3	6,6,open	3.86	0.067		
			8.2,[d] 3.8[d]	0.143, 0.066		

[a] Reference 16 Lu, X. et al. *J. Am. Chem. Soc.* **2004**, *126*, 14871−14878. [b] Reference 2 Niyogi, S. et al. *Acc. Chem. Res.* **2002**, *35*, 1105−1113. [c] Reference 17 Hamon, M. A. et al. *J. Am. Chem. Soc.* **2001**, *123*, 11292-1293. [d] Reference 18 Haddon, R. C. *J. Am. Chem. Soc.* **1987**, *109*, 1676.

respectively. Figure 1o represents for the side view and Figure 1p for the top view of model **$C_{20}H_{10}$**, a bowl-shape molecule.

For simplicity, the calculations of the energies of the transition states (TS) and the reaction barriers (except for C_{60}) are neglected in spite of their importance in reality. The TS search and optimization are time intensive if using high-level DFT methods for systems with hundreds of atoms. A comparison of the reactivity of different sites on a fullerene or a nanotube was preferably studied. Nevertheless, without the calculations of barriers, it will not affect the comparison. The fragments $-HNCH_3$ and $-H$ are added via a bond on fullerenes or onto various locations of the nanotubes (caps, sidewalls, and defects). The structures of reactants and possible products (and their isomers) were fully optimized by quantum mechanics methods on the basis of density functional theory (DFT) in the generalized gradient approximation with nonlocal exchange and correlation functions according to Perdew and Wang (GGA-PW91).[15] The DFT calculations were performed using the DMol^3 module in the Materials Studio (MS) Modeling software package (Accelrys Inc.).[13,14] The convergence thresholds for

TABLE 2: The Reaction Energies: Calculated Relative Energies (kcal/mol) for the Final Products Referred to the Reactants Species

addition sites iN-jH[b]	type of bond via m,n-membered rings fusion bond, location, bond orientation relative to the tube axis	reaction energy DMol[3] PW91/DNP (fine)	formation energy refs	addition sites initial angles (referred toTable 1) θ_{pi}	θ_{pj}	$\phi_{i,j}$
		$C_{60}(I_h)$				
			B3LYP/STO-3G[a]			
1N-6H (Figure 1j)	5,6 bond	14.0	−1.7	11.64	11.64	0
1N-6H (Figure 1k)	6,6 bond	−2.9	−23.0	11.64	11.64	0
		5_5_capsC_{140} (Figure 1a and 1b)				
			AM1[b]			
1N-2H	5,6 bond, caps	12.6	−4.2	11.89	11.86	0.03
1N-3H	6,6 bond, caps	−2.7	−22.9	11.89	12.12	0
3N-1H	6,6 bond, caps	−1.2	−22.9	12.12	11.89	0
3N-4H	5,6 bond, caps	13.1	−4	12.12	11.66	0.27
4N-3H	5,6 bond, caps	11.9	−3.5	11.66	12.12	0.27
4N-5H	6,6 bond, caps	0.6	−19.7	11.66	11.63	0.04
4N-6H	5,6 bond, caps	12.2	−5.2	11.66	10.42	2.25
6N-4H	5,6 bond, caps	13.3	−3.9	10.42	11.66	2.25
6N-7H	5,6 bond, caps	8.4	0.4	10.42	10.45	0.02
6N-8H	6,6 bond, caps	12.1	−6.5	10.42	7.41	10.19
8N-6H	6,6 bond, caps	12.7	−2.8	7.41	10.42	10.19
8N-9H	6,6 bond, sidewalls, perpendicular	30.3	26.4	7.41	7.44	0.02
8N-10H	6,6 bond, sidewalls, diagonal	23.3	22.4	7.41	5.77	18.68
10N-8H	6,6 bond, sidewalls, diagonal	25.3	25.4	5.77	7.41	18.68
10N-11H	6,6 bond, sidewalls, perpendicular	24.1	17.3	5.77	5.87	0.02
10N-12H	6,6 bond, sidewalls, diagonal	25.9	21.2	5.77	5.82	21.49
12N-10H	6,6 bond, sidewalls, diagonal	26.3	21.5	5.82	5.77	21.49
12N-13H	6,6 bond, sidewalls, perpendicular	24.1	30.7	5.82	5.70	0.02
		10_0_cap$C_{100}H_{10}$ (Figure 1d and 1e)				
			AM1[b]			
1N-2H	5,6 bond, the cap	−1.5	−30.4	10.58	10.60	0
1N-3H	6,6 bond, the cap	12.4	−13.6	10.58	9.06	0
3N-1H	6,6 bond, the cap	10.9	−11.4	9.06	10.58	0
3N-4H	6,6 bond, the cap	14.0	−7.6	9.06	10.76	−0.35
4N-3H	6,6 bond, the cap	13.5	−8.5	10.76	9.06	−0.35
4N-5H	5,6 bond, the cap	−2.1	−26.5	10.76	10.76	0.03
4N-6H	5,6 bond, the cap	−1.5	−26.7	10.76	10.79	−0.79
6N-4H	5,6 bond, the cap	−1.6	−26.5	10.79	10.76	−0.79
6N-7H	5,6 bond, the cap	6.0	−8.0	10.79	9.20	3.30
7N-6H	5,6 bond, the cap	6.1	−6.5	9.20	10.79	3.30
7N-8H	6,6 bond, the cap	14.8	18.5	9.20	6.97	0.06
8N-7H	6,6 bond, the cap	15.2	19.2	6.97	9.20	0.06
8N-9H	6,6 bond, sidewalls, diagonal	25.8	11.3	6.97	4.88	−17.21
9N-8H	6,6 bond, sidewalls, diagonal	25.4	13.3	4.88	6.97	−17.21
9N-10H	6,6 bond, sidewalls, parallel	26.6		4.88	5.02	0.58
10N-9H	6,6 bond, sidewalls, parallel	29.6		5.02	4.88	0.58
10N-11H	6,6 bond, sidewalls, diagonal	25.0		5.02	4.65	−18.61
11N-10H	6,6 bond, sidewalls, diagonal	24.8		4.65	5.02	−18.61
		5_5$C_{140}H_{20}$ (Figure 1c)				
2N-1H	6,6 bond, sidewalls, diagonal	26.5		5.98	5.93	21.12
2N-3H	6,6 bond, sidewalls, perpendicular	27.4		5.98	5.85	−0.01
		10_0$C_{160}H_{20}$ (Figure 1f)				
2N-3H	6,6 bond, sidewalls, parallel	27.1		5.18	5.18	0
2N-1H	6,6 bond, sidewalls, diagonal	32.6		5.18	5.20	18.00
		10_0_capsC_{160} (Figure 1g and 1h)				
1N-2H	5,6 bond, caps	−4.3		10.59	10.60	−0.01
1N-3H	6,6 bond, caps	14.5		10.59	8.92	0.02
		5_5_d1 (7−5−5−7 defect) (Figure 1i)				
1N-2H	5,5 bond, a 7−5−5−7 defect on sidewalls	−33.3		15.8	15.8	0
		5_5_kink (Figure 1l)				
1N-2H	5,6 bond, a defect at the joint	−12.1		16.30	12.98	6.13
1N-3H	5,5 bond, a defect at the joint	−20.8		16.30	16.30	0.04
		$C_{50}(D_{5h})$ (Figure 1m)				
1N-2H	5,5 bond	−31.6		15.60	15.53	0.01
		$C_{50}(D_3)$ (Figure 1n)				
1N-2H	5,5 bond	−9.3		15.21	14.15	1.98
		$C_{20}H_{10}$(bowl) (Figure 1o and 1p)				
1N-2H	5,6 bond	25.6		8.34	8.34	0.01
1N-3H	6,6 bond	24.9		8.34	3.86	0.12

[a] Reference 11 Basiuk, E. V. et al. *Carbon* **2003**, *41*, 2339−2346. [b] Reference 12 Basiuk, E. V. et al. *Nano Lett.* **2004**, *4*, 863−866.

energy change, maximum force, and maximum displacement between optimization cycles are set to 10^{-5} Hartree, 0.002 Hartree/Å, and 0.005 Å, respectively. SCF density convergence is 10^{-6}. The orbital cutoff is 3.7 Å. The reaction energy is evaluated as the total energy difference between the product and the reactants. If the reaction energy is negative (positive), the reaction is exothermic (endothermic). The reaction energy is one of the indexes of chemical reactivity.

In the DMol[3] code, each electronic wave function is expanded in a localized atom-centered basis with each basis function defined numerically on a dense radial grid. The selected basis set is DNP, a double-numerical with polarization functions basis set. It is one of the most complete sets available in the code. The size of the DNP set is comparable to Gaussian basis set 6-31G**. The use of the exact DFT spherical atomic orbitals has several advantages. For one, the molecule can be dissociated exactly to its constituent atoms (within the DFT context). Because of the quality of these orbitals, basis set superposition effects are minimized[13] and it is possible to obtain an excellent description, even for weak bonds. All geometric optimization jobs were run in parallel on a SGI server.

Results and Discussion

Topological analyses of the DFT (GGA-PW91/DNP) fully optimized geometric structures are summarized in Table 1. The atomic numbering schemes are shown in Figure 1. The pyramidalization angles obtained are 11.64° for any carbon atoms of $C_{60}(I_h)$, 15.56° for the carbon atoms at the equator of $C_{50}(D_{5h})$, and 15.21° and 14.15° for the carbon atoms at the 5,5 bonds of $C_{50}(D_3)$. These angles are in good agreement with the B3LYP/6-31G* results[16] calculated using the Gaussian98 program. The pyramidalization angle θ_p and the π-orbital misalignment angle ϕ on the perfect sidewalls of the carbon nanotubes are $\theta_p \sim 5.92°$ (on average) and $\phi \sim 0°$ and 21.12° for the (5,5) tube (model **5_5C$_{140}$H$_{20}$**), $\theta_p \sim 5.18°$ (on average) and $\phi \sim 0°$ and 18° for the (10,0) tube (model **10_0C$_{160}$H$_{20}$**), and $\theta_p \sim 8.34°$ and 3.86° for the bowl-shaped molecule (model **C$_{20}$H$_{10}$**), respectively. All these angles are consistent with Haddon and co-workers' results.[17,18,2] The pyramidalization angle θ_p of a carbon atom at a vertex formed with three polygons is listed in order: θ_p (five-, five-, six-membered rings vertex or five-, five-, seven-membered rings vertex) > θ_p (five-, six-, six-membered rings vertex) > θ_p (six-, six-, six-membered rings vertex). In other words, the θ_p decreases in sequence at the site with two pentagons, only one pentagon, and no pentagons. The carbon atoms with maximum pyramidalization angle are invariably located at five-membered rings. All the carbon atoms on a perfect sidewall of pristine nanotubes (5,5) and (10,0) are located at sites formed with six-, six-, six-membered rings. Moreover, the θ_p of the (5,5) tube is slightly larger than that of the (10,0) tube because the (5,5) tube has a smaller diameter (6.76 Å) than that of the (10,0) tube (7.81 Å).[2] In the capped nanotube models, the θ_p decreases gradually from the tip of caps (which is close to C_{60}) to the sidewall.

The calculated reaction energies are listed in the third column of Table 2. Some corresponding B3LYP/STO-3G and AM1 results[11,12] are cited in the fourth column of Table 2. The first column shows (following the conventions of ref 12) the notation of the addition site positions: iN-jH, where "N" and "H" denote the sites of C_{SWNT}-$NHCH_3$ ($C_{fullerene}$-$NHCH_3$) and C_{SWNT}-H ($C_{fullerene}$-H) bond formations, respectively; i and j correspond to the numbering schemes as shown in Figure 1. For the convenience of comparing the reactivity of different sites, the type, location, and orientation (relative to the nanotube axis) are indicated in the second column of Table 2. To correlate the reactivity of sites to their topology, the initial pyramidalization angles $(\theta_p)_i$, $(\theta_p)_j$, and the initial π-orbital misalignment angle ϕ_{ij} of the two carbon atoms (labeled as i and j) at the bond were analyzed and listed in last three columns of Table 2, respectively.

It can be seen from Table 2 that the most exothermic and active sites are located at the 5,5 bonds. For example, the reaction energy for methylamine addition is −31.6 kcal/mol via the equatorial pentagon−pentagon fusion bond of a C_{50} with symmetry D_{5h}, −33.3 kcal/mol via the 5,5 bond at a pentagon−heptagon (7−5−5−7) defect on the nanotube sidewall, and −20.8 kcal/mol via the 5,5 bond at the junction of two nanotubes. Further analysis found that pyramidalization angles of carbon atoms at these sites are very large (normally greater than fifteen degrees), and thus great strain energies have been accumulated at the sites before the addition reaction. Therefore, these carbon atoms have high reactivity and can be transferred to tetrahedral sp^3-hybridized carbon atoms easily. Similar analysis revealed that the average pyramidalization angles on caps (>7°) are larger than those on the sidewall (<7°). As a result, the reactivity on caps was higher (the reaction energy is 15−30 kcal/mol less) compared to that on the sidewall. At the tip sites of the cap of the (5,5) nanotube, the addition of methylamine via the 6,6 bond even exhibits a little exothermic (−2.7 kcal/mol) and more favorable than via the 5,6 bond (12.6 kcal/mol), which is similar to the trend of the addition to C_{60}, −2.9 kcal/mol via the 6,6 bond and 14.0 kcal/mol via the 5,6 bond. On the contrary, for the (10,0) nanotube, reaction via the 5,6 bond (−1.5 kcal/mol for model **10_0_capC$_{100}$H$_{10}$** and −4.3 kcal/mol for model **10_0_capsC$_{160}$**) is energetically more favorable than via the 6,6 bond (12.4 kcal/mol for model **10_0_capC$_{100}$H$_{10}$** and 14.5 kcal/mol for model **10_0_capC$_{100}$H$_{10}$**). The pyramidalization angles are almost the same at these sites. The results clearly indicate that the reactivity may arise from other reasons except for the topology.

The relative reactivity of sites in general is consistent with the B3LYP/STO-3G and AM1 results.[11,12] Carbon nanotubes are reactive at their end caps. However, the reaction on C_{60} or at caps of nanotubes are not as exothermic as those indicated in the B3LYP/STO-3G and AM1 results.[11,12] In addition, probable reaction sites were also found at the defect sites or kink sites, which was in agreement with the observations in experiments.[12]

Conclusion

High-level DFT computations have been carried out to study the relationship between reactivity and curvature for the addition of methylamine onto the strained molecules: the fullerenes C_{50} and C_{60} or the carbon nanotubes (5,5) and (10,0). It was found that the carbon atoms with large values of θ_p exhibit high reactivity. The most energetically favorable sites are found at the pentagon−pentagon fusions on C_{50}, the 7−5−5−7 defect on the sidewall of a nanotube, or the junction of two nanotubes. The enhanced reactivity of the end caps and defect sites compared to that of the sidewall can be explained by the increased strain at these sites that causes a partial loss of conjugation.

References and Notes

(1) Sun, Y. P.; Fu, K.; Lin, Y.; Huang, W. *Acc. Chem. Res.* **2002**, *35*, 1096.

(2) Niyogi, S.; Hamon, M. A.; Hu, H.; Zhao, B.; Bhowmick, P.; Sen, R.; Itkis, M. E.; Haddon, R. C. *Acc. Chem. Res.* **2002**, *35*, 1105.

(3) Haddon, R. C.; Scott, L. T. *Pure Appl. Chem.* **1986**, *58*, 137.

(4) Haddon, R. C. *Science* **1993**, *261*, 1545.
(5) Haddon, R. C. *J. Am. Chem. Soc.* **1997**, *119*, 1797.
(6) Klein, D. J.; Liu, X. *Int. J. Quantum Chem.* **1994**, *52* (S28), 501.
(7) Schmalz, T. G.; Seitz, W. A.; Klein, D. J.; Hite, G. E. *J. Am. Chem. Soc.* **1988**, *110*, 1113.
(8) Bakowies, D.; Thiel, W. *J. Am. Chem. Soc.* **1991**, *113*, 3704.
(9) Kar, T.; Akdim, B.; Duan, X.; Pachter, R. *Chem. Phys. Lett.* **2004**, *392*, 176.
(10) Akdim, B.; Kar, T.; Duan, X.; Pachter, R. Functionalization of Single-Wall Carbon Nanotubes: An Assessment of Computational Methods. In *Computational Science, Lecture Notes in Computer Science*; *9*, Springer-Verlag: New York, 2004; Vol. *303*.
(11) Basiuk, E. V.; Basiuk, V. A.; Shabel'nikov, V. P.; Golovatyi, V. G.; Flores, J. O.; Saniger, J. M. *Carbon* **2003**, *41*, 2339.
(12) Basiuk, E. V.; Monroy-Pelaez, M.; Puente-Lee, I.; Basiuk, V. A. *Nano Lett.* **2004**, *4*, 863.
(13) Delley, B. *J. Chem. Phys.* **1990**, *92*, 508.
(14) Delley, B. *J. Chem. Phys.* **2000**, *113*, 7756.
(15) Perdew, J. P.; Wang, Y. *Phys. Rev. B* **1992**, *45*, 13244.
(16) Lu, X.; Chen, Z.; Thiel, W.; Schleyer, P. von R.; Huang, R.; Zheng, L. *J. Am. Chem. Soc.* **2004**, *126*, 14871.
(17) Hamon, M. A.; Itkis, M. E.; Niyogi, S.; Alvaraez, T.; Kuper, C.; Menon, M.; Haddon, R. C. *J. Am. Chem.* Soc. **2001**, *123*, 11292.
(18) Haddon, R. C. *J. Am. Chem. Soc.* **1987**, *109*, 1676.